Supplementary Information:

Model Details

The model used in this study is fully described by previous work [English et al., 2011] except that these simulations also include an input of meteoritic smoke along with the full sulfate aerosol microphysics and chemistry. The meteoritic material was shown to play a significant role in the composition of aerosol through out the stratosphere [Murphy et al., 1998, 2007]. A recent study has also shown that meteoritic smoke is important to include in studies of stratospheric extinction that examine the upper stratosphere, particularly studies which involve lidar observations [Neely III et al., 2011].

Central to the experiment are the sources of SO_2 involved in the two theories attempting to explain the increases in stratospheric aerosol from 2000 to 2010. To that end, great care was taken to accurately depict the contribution of SO_2 from both anthropogenic and volcanic emissions as described in detail below.

Modeling Anthropogenic SO_2 Emissions

To isolate and represent the trends in anthropogenic emissions thought to be important for trends in stratospheric aerosol an emission scheme was created that added the increases in Chinese and Indian SO_2 to the 2-d baseline model emissions that are representative of the year 2000 [Hofmann et al., 2009; Smith et al., 2011; Lu et al., 2010, 2011]. For reference, in 2000 annual SO_2 emissions in China and India totaled ~21 Tg and ~5.8 Tg, respectively [Smith et al., 2011; Lu et al., 2010, 2011]. The increases were determined from observations and inventories [Lu et al., 2010, 2011]. To create the

increased emissions in the model, the emissions in the grid squares representing the industrial regions in China and India are multiplied by a factor at each time step that resulted in a total annual emission matching the reported annual emissions for the year of interest. Once this model input was created, another simulation was conducted in which the increases in Chinese and Indian emissions were multiplied by a factor of ten. It is highly unlikely that emissions would ever reach values as large as ten times the current levels. The factor of ten was chosen so that the effect of the Asian emissions on the stratospheric aerosol could be easily seen in the simulations. The yearly total additional (above 2000 levels) emissios of SO_2 added to the actual anthropogenic increased emission model runs is shown in Figure S1.

Besides the important chemistry and microphysics, accurate transport mechanisms are key to simulating the impact our surface emissions on the stratosphere. Monthly mean CO mixing ratios from the WACCM simulations at 100 hPa are compared to the MLS CO measurements in Figure S2 for June 2005. The CO used here are based on MLS observations from retrieval version 3.3 (v3.3) [Pumphrey et al., 2007; Livesey et al., 2011]. MLS (Fig. S2a) shows a maximum in CO over the area associated with Asian monsoon anticyclone at 100 hPa [Park et al, 2009]. CO from WACCM (Fig. S2a) shows an overall agreement of this pattern, though WACCM shows a reduced magnitude. This could be due to low emission sources in the model or the differences may be due to the ±20 ppbv and ±30% systemic uncertainty of MLS at this level [Park et al, 2009; Livesey et al., 2011]. Figure S2 also displays the concentration of CO on the eastern (Fig. S2c) and western (Fig. S2d) sides of the monsoon region from the WACCM simulations. In comparison to other studies using chemical transport models, Fig. S2c and d demonstrate

that the model used in this study has a vertical structure similar to that observed in CO and other tropospheric tracers inside the anticyclone. Specifically, the ratio of the amount of CO at the surface to that in the upper atmosphere, as compared to observations and other modeling studies, suggest our simulation adequately represent the vertical transport in this region [Park et al, 2009].

Figure S3 displays a comparison of the zonally averaged vertical distribution of SO_2 in the tropics from a baseline simulation, an increased Asian emission simulation and the ten times (10x) increased Asian emission simulation. The simulated Manam volcanic injection is also shown as a juxtaposition of the emission types (surface source versus direct stratospheric injection). The increased Asian emissions elevate the SO_2 burden from 4 km to 18 km by ~20%. Above 18 km, no difference in the SO_2 burden is discernable between the baseline emissions and the increased Asian emission simulations. The 10x Asian emissions run increases the lower tropospheric burden even further but matches the simulation using the baseline emissions above 16 km. Tropospheric SO_2 is largely converted to sulfuric acid vapor and then to sulfates in the upper troposphere, and influences the stratosphere indirectly though transport of the sulfates across the tropopause. In contrast the volcanic injection significantly influences the SO_2 profile in the lower stratosphere, because the SO_2 is directly injected there. (Note Fig. S2 shows the volcanic injection directly above the volcano on the day of the eruption, so it is not strictly comparable to the other plots, which are zonal and monthly means). Above the injection region (~22 km) the SO_2 concentrations are undisturbed.

Modeling Volcanic Injections of SO_2

To simulate the volcanic eruptions from 2000 to 2010 that impacted stratospheric aerosol formation, an inventory was made of all the volcanoes with volcanic explosivity index (VEI) of 3 or greater during this period [Newhall and Self, 1982]. The information used to model the volcanoes was gathered from various peer reviewed publications and the Smithsonian's Global Volcanism Program's reports for each eruption (http://www.volcano.si.edu/reports/usgs/). These reports contain information about the injection height and the amount of SO_2 for each injection. The amount of SO_2 injected was measured from satellite observations. An example of the SO_2 observations used is seen in Figure S4. A summary of the data for each volcano may be found in Table S1. Using this information, each volcanic eruption was assigned an injection height and amount of total emitted SO_2. The location of each injection was modeled at the corresponding model grid cell, which included the volcano. The vertical distribution of SO_2 was simulated as a Gaussian shaped plume with a maximum emission at the model level most closely matching the observed injection height and the full injection spread over 5 model levels (~4-6 km). The Gaussian injection profile is supported by recent observations of the SO_2 profile following the Sarychev eruption [Doeringer et al., 2012]. This work shows that the majority of the SO_2 produced by the Sarychev eruption in 2009 forms a Gaussian shaped plume centered near the region of highest aerosol extinction observed just after the eruption [Doeringer et al., 2012]. No constraint, except for the profile and flux of SO_2 during the initial injection (typically lasting 6 model hours) is placed on the volcanic plume. Thus, the SO_2 is transported according to the dynamics of

the model and the resulting sulfate aerosol evolves freely from this source as defined by the chemical and microphysical schemes represented in the model.

It should be noted that some of the studies cited for the volcanic injection parameters in Table S1 use observations from CALIOP and SAGE II, which would seem to make the comparison in Figures 1 circular. These observations, particularly the information about the height of the injection, have been corroborated with observations from the ground and aircraft as reported from the Smithsonian Global Volcanism Program. In either case, these observations are based on observations that rely on light scattering from the particulates and clouds associated with the plume of eruption. Even with current abilities to measure SO_2 profiles, these same clouds obscure the ability to accurately make limb observations of SO_2. As such few direct observations of SO_2 profiles of a volcanic eruption have been made with the necessary vertical resolution to be used as the only source of information to base the simulations upon [Doeringer et al., 2012]. The few observations published that show profiles of extinction and SO_2 soon after a volcanic eruption and the modeling work that describes the path of the plume of SO_2 after the Soufriére Hills eruption in 2006 suggest that the observations used here as basis for the simulations are appropriate [Doeringer et al., 2012; Prata et al., 2007]. Also, because the injections consist only of SO_2, not sulfate aerosol, we believe the comparison to be fair for the purpose of this study.

Model Optical Calculations

To compare the model output to the observations, aerosol extinction was calculated from the model's size distributions of pure sulfate, meteoritic and mixed (sulfate with meteoritic core) aerosol using Mie scattering theory adapted for use in MATLAB [Bohren and Huffman, 1983; Mätzler, 2002].

For the pure sulfate and mixed sulfate aerosol, the particles were assumed to be spherical and, for particles with a meteoritic core, the core was assumed to be optically identical to the sulfate. Thus, the optical calculations of the modeled sulfate aerosol ignore absorption, which may cause an under-estimation of their true extinction. It is suspected that the cores are often dissolved in the sulfuric acid, so the approximation should be fairly accurate. The real component was allowed to vary as a function of the mass percent of H_2SO_4 present within the aerosol as described by previous studies [Palmer and Williams, 1975]. The data was linearly interpolated so that a continuous function for the index of refraction as a function of the mass percent of H_2SO_4 could be made and used to determine the index of refraction for the complete range of concentration values found in the aerosol within the model. The index of refraction of the aerosol should also be a function of temperature and pressure, but for the wavelength of the observations examined here (525 nm) the variation is small compared to that caused by the variation in H_2SO_4 content [Massie, 1994; Muller et al., 1999; Redemann et al., 2000; Myhre et al., 2003; Zhao et al., 1997].

Other Sources of Stratospheric Aerosol Variability

Pyrocumulonimbus (pyroCb) events are similar in nature (but in most cases smaller in magnitude) to volcanic injection of aerosol to the stratosphere [Fromm et al, 2008]. For the purposes of this work the injections are acknowledged as another source of variability in the aerosol record, but are not dealt with directly because their ability to impact the middle and upper stratosphere optical depth (above 20 km) is negligible [Fromm et al, 2008]. A recent study shows that even the massive Victoria, Australia fire in February 2009 had minimal impact on the stratospheric optical depth in comparison to the volcanic eruptions from 2000 to 2010 [Vernier et al., 2011]. More observations of pyroCb will be needed before they can be analyzed with simulations similar to those in this work. Despite the lower optical depth of the carbonaceous material, it is possible it might alter the ability of the stratospheric aerosol to absorb light.

It has also been suggested that the stratospheric circulation has been impacted by greenhouse gas warming [Butchart et al., 2010]. If the cross-tropopause upward flux of tropical air has increased, it will loft more aerosol and aerosol precursors into the stratosphere, causing an upward aerosol trend. In the absence of compensating radiative processes, an increase in the upward flux of tropical air would also cause a decrease in tropical tropopause temperatures, which could increase nucleation rates of sulfate aerosol at the point of injection into the stratosphere [Butchart et al., 2010; Hamill et al., 1997; Yue and Deepak, 1982; Rosenlof and Reid, 2008]. However, there is evidence that argues that the properties of the aerosol in the upper troposphere and lower stratosphere at not very sensitive to the nucleation rate [English et al., 2011]. This process is not examined in this work.

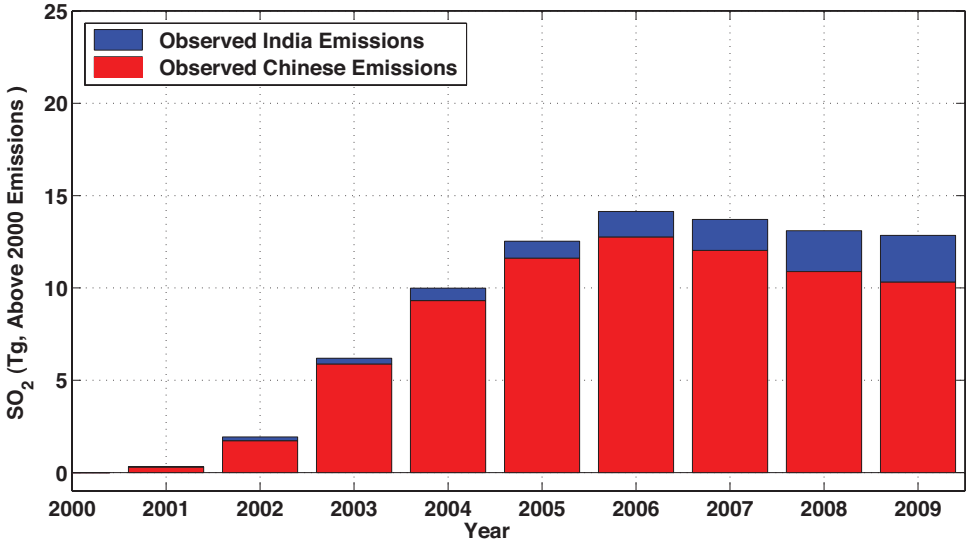

Figure S1. Yearly observed Chinese and Indian emissions from 2000 to 2010. The bars represent the increases (above 2000 levels [Smith et al., 2011; Lu et al., 2010, 2011]) of anthropogenic emissions of SO_2 from China and India from 2000 to 2010 [Lu et al., 2010, 2011].

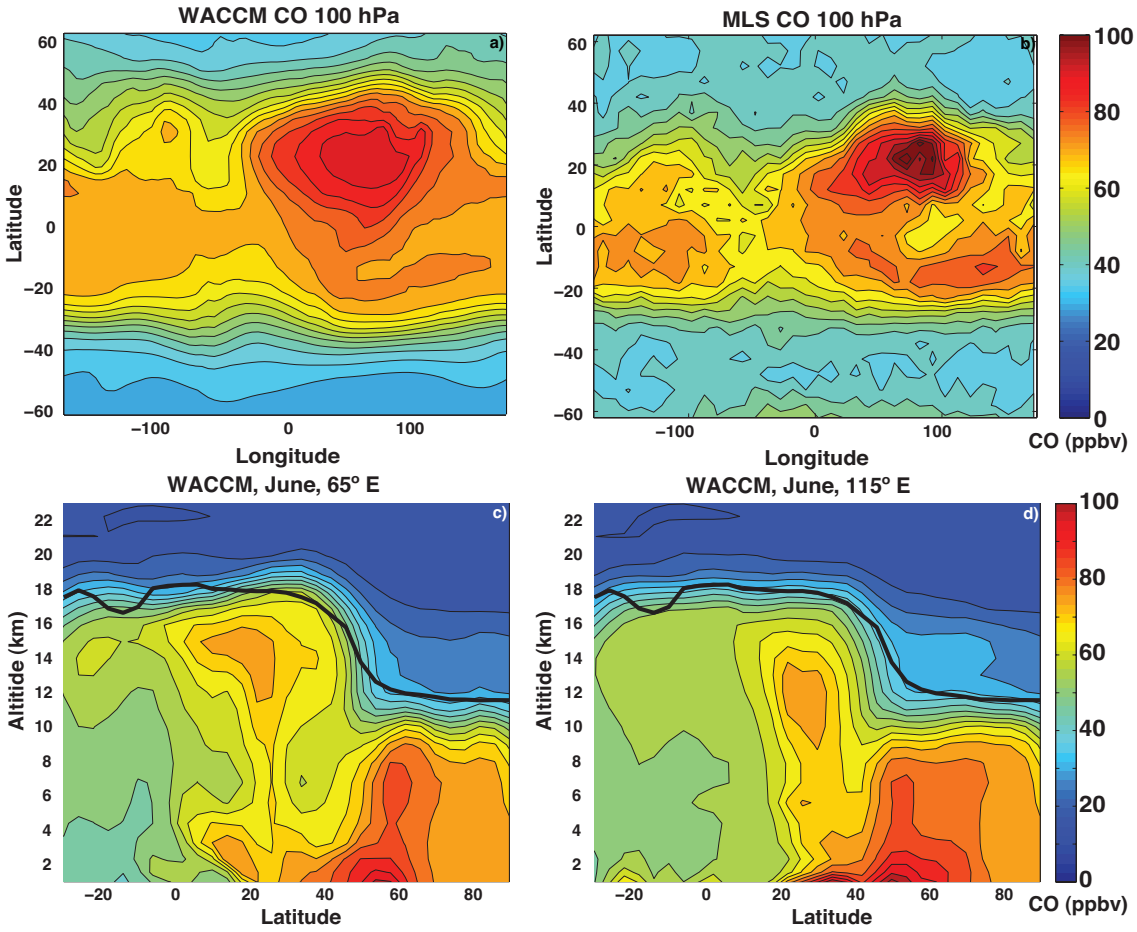

Figure S2. Validation of model transport characteristics using CO as a tracer. Plots at 100 hPa of CO from WACCM (a) and MLS (b) and latitude-altitude cross-sections of monthly mean WACCM CO at the (c) western (65°E) and (d) eastern (115°E) edges of the Asian monsoon maximum in the model month of June 2005. Thermal tropopause derived from the model temperature profile is denoted as thick black lines.

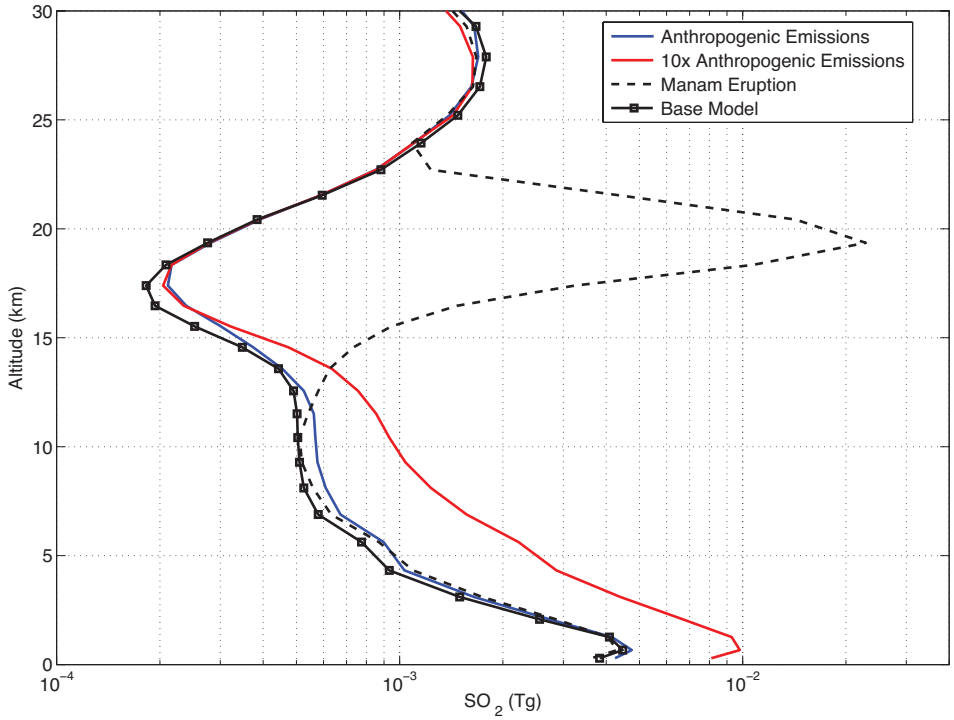

Figure S3. Example SO_2 profiles from model. Zonal, monthly mean SO_2 profiles from 2°S to 2°N during model month 61 (simulated January, 2005 and also month of Manam eruption). The volcanic profile (black dashed line) is taken over the grid column containing Manam on the day of the eruption. The black solid line is from a baseline emission model run. The blue line is from a simulation with increased Asian SO_2 emissions from 2000-2010 as illustrated in Fig. S1. The red line is from the simulation with ten times the observed increase in Asian SO_2 emissions.

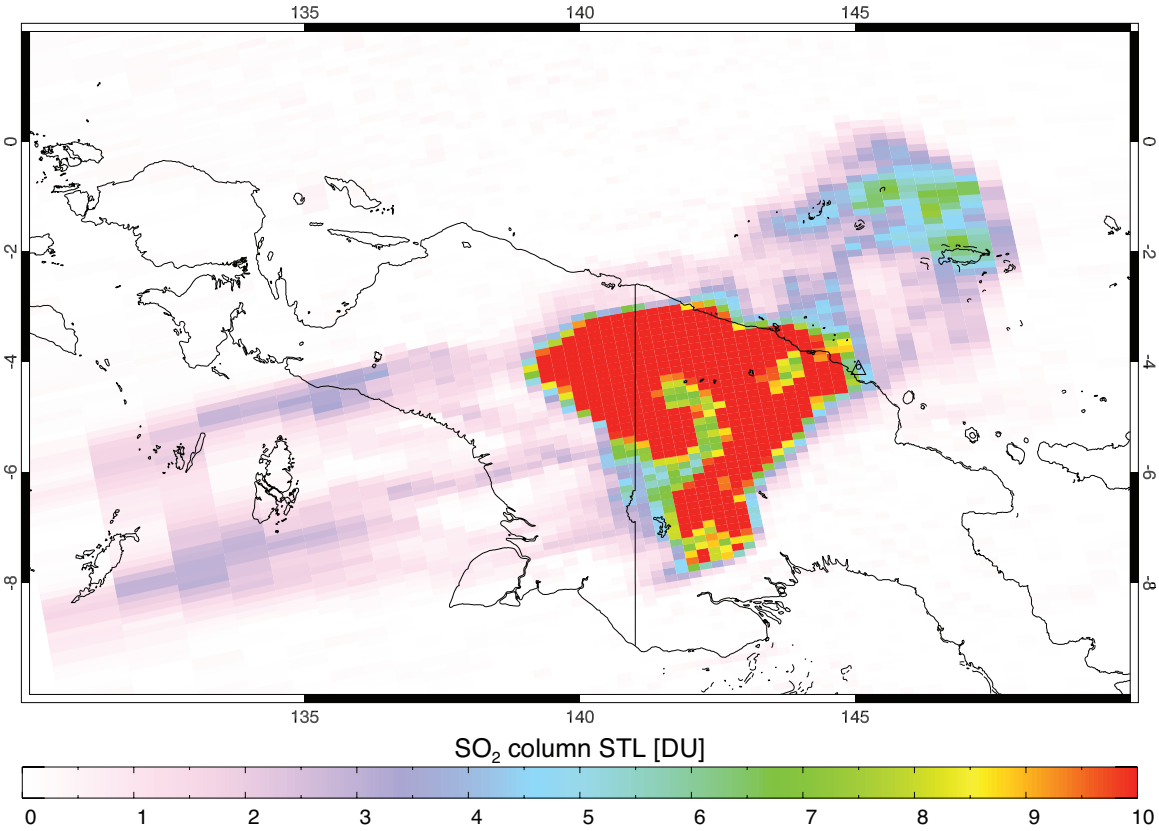

Figure S4. Example satellite observation of volcanic SO_2. Total column SO_2 observed on 28 January 2005 (one day after the original eruption) by the Ozone Monitoring Instrument (OMI) on board the EOS/Aura satellite platform. This and other volcanic SO_2 data is available at: http://so2.gsfc.nasa.gov.

Table S1. Summary of volcanic eruption simulation parameters. Volcanic emission database used for simulations eruptions. Parameters were derived from information gathered by the Global Volcanism Program (maintained by the Smithsonian Institution) and the citations shown. Eruption dates are represented in decimal year. If multiple heights were reported, we used the ones denoted by an * in our simulations.

Volcano	Eruption Date	Lat.	Long.	SO_2 Injected (Tg)	Max. Injection Height (km)	VEI
Ulawun (Ul)	2000.74	-5	151	0.05 [Deshler et al., 2006]	15	4
Ruang (Ru)	2002.73	2	125	0.055 [Prata and Bernardo, 2007]	20 [Prata and Bernardo, 2007] 16* [Tupper et al., 2007]	4
Reventador (Ra)	2002.83	0	-78	0.096 [Carn et al., 2009]	17	4
Anatahan (At)	2004.28	16	146	0.065 [Prata and Bernardo, 2007]	15 [Prata and Bernardo, 2007]	3
Manam (Ma)	2005.07	-4	145	0.18 [Prata and Bernardo, 2007]	19 [Kamei et al., 2006]	4
Sierra Negra (Si)	2005.81	1	91	0.36 [Thomas et al., 2009]	15 [Thomas et al., 2009; Geist et al., 2007]	3
Soufrière Hills (So)	2006.38	16	-62	0.2 [Prata and Bernardo, 2007]	20 [Prata and Bernardo, 2007]	3
Tavurvur (Ta)	2006.76	-4	152	0.125 [Prata and Bernardo, 2007]	17 [Prata and Bernardo, 2007]	4
Jebel at Tair (Jb)	2007.75	16	42	0.08 [Carn et al., 2009]	16 [Carn et al., 2009]	3
Chaiten (Ch)	2008.34	-43	-73	0.01 [Carn et al., 2009]	19* [Carn et al., 2009]	4
Okmok (Ok)	2008.53	53	-168	0.122 [Prata et al., 2010]	16 [Arnoult et al., 2010]	4
Kasatochi (Ka)	2008.60	52	-176	1.7 [Corradini et al., 2010]	14-18 [Waythomas et al., 2010] 18* [Bitar et al., 2010]	4
Sarychev (Sa)	2009.44	48	153	1.4 [O'Neill et al., 2012]	17 [O'Neill et al., 2012]	4

References for Supplementary Information

Arnoult, K., J. Olson, C. Szuberla, S. McNutt, M. Garcés, D. Fee, and M. Hedlin (2010), Infrasound observations of the 2008 explosive eruptions of Okmok and Kasatochi volcanoes, *J. Geophys. Res*, *115*, D00L15, doi:10.1029/2010JD013987.

Bitar, L., T. J. Duck, N. I. Kristiansen, A. Stohl, and S. Beauchamp (2010), Lidar observations of Kasatochi volcano aerosols in the troposphere and stratosphere, *J. Geophys. Res*, *115*(D2), D00L13–, doi:10.1029/2009JD013650.

Bohren, C., and D. Huffman (1983), *Absorption and scattering of light by small particles*, Wiley-Interscience.

Butchart, N., I. Cionni, V. Eyring, T. Shepherd, D. Waugh, H. Akiyoshi, J. Austin, C. Brühl, M. Chipperfield, and E. Cordero (2010), Chemistry-Climate Model Simulations of Twenty-First Century Stratospheric Climate and Circulation Changes, *Journal of Climate*, *23*(20), 5349–5374, doi:10.1175/2010JCLI3404.1.

Carn, S. A., A. J. Krueger, N. A. Krotkov, K. Yang, and K. Evans (2009), Tracking volcanic sulfur dioxide clouds for aviation hazard mitigation, *Nat Hazards*, *51*(2), 325–343, doi:10.1007/s11069-008-9228-4.

Corradini, S., L. Merucci, A. Prata, and A. Piscini (2010), Volcanic ash and SO2 in the 2008 Kasatochi eruption: Retrievals comparison from different IR satellite sensors, *J. Geophys. Res*, *115*, D00L21, doi:10.1029/2009JD013634.

Deshler, T., R. Anderson-Sprecher, H. Jäger, J. Barnes, D. J. Hofmann, B. Clemesha, D. Simonich, M. Osborn, R. Grainger, and S. Godin-Beekmann (2006), Trends in the nonvolcanic component of stratospheric aerosol over the period 1971–2004, *J. Geophys. Res*, *111*, D01201, doi:10.1029/2005JD006089.

Doeringer, D., A. Eldering, C. D. Boone, G. González Abad, and P. F. Bernath (2012), Observation of sulfate aerosols and SO 2from the Sarychev volcanic eruption using data from the Atmospheric Chemistry Experiment (ACE), *J. Geophys. Res*, *117*(D3), D03203–, doi:10.1029/2011JD016556.

English, J., O. Toon, and M. Mills (2011), Microphysical simulations of new particle formation in the upper troposphere and lower stratosphere, *Atmopsheric Chemistry and Physics*, *11*, 12441–12486, doi:10.5194/acpd-11-12441-2011.

Fromm, M., O. Torres, D. Diner, D. Lindsey, Hull, B.V., R. Servranckx, E. Shettle, and Z. Li (2008), Stratospheric impact of the Chisholm pyrocumulonimbus eruption: 1. Earth-viewing satellite perspective, *J. Geophys. Res*, *113*, D08202, doi:10.1029/2007JD009147.

Geist, D. J., K. S. Harpp, T. R. Naumann, M. Poland, W. W. Chadwick, M. Hall, and E. Rader (2007), The 2005 eruption of Sierra Negra volcano, Galápagos, Ecuador, *Bull Volcanol*, *70*(6), 655–673, doi:10.1007/s00445-007-0160-3.

Hamill, P., E. J. Jensen, P. Russell, and J. J. Bauman (1997), The life cycle of stratospheric aerosol particles, *Bulletin of the American Meteorological Society*, *78*(7), 1395–1410.

Hofmann, D., J. Barnes, M. O'Neill, M. Trudeau, and R. Neely (2009), Increase in background stratospheric aerosol observed with lidar at Mauna Loa Observatory and Boulder, Colorado, *Geophys. Res. Lett*, *36*(15), 1–5.

Kamei, A., N. Sugimoto, I. Matsui, A. Shimizu, and T. Shibata (2006), Volcanic Aerosol Layer Observed by Shipboard Lidar over the Tropical Western Pacific, *SOLA*, *2*, 1–4, doi:10.2151/sola.2006-001.

Livesey, N. J. et al. (2011), *Earth Observing System (EOS) Aura Microwave Limb Sounder (MLS) Version 3.3 Level 2 data quality and description document*., NASA Jet Propulsion Laboratory California Institute of Technology, Pasadena, California, 91109-8099.

Lu, Z., D. G. Streets, Q. Zhang, S. Wang, G. R. Carmichael, Y. F. Cheng, C. Wei, M. Chin, T. Diehl, and Q. Tan (2010), Sulfur dioxide emissions in China and sulfur trends in East Asia since 2000, *Atmos. Chem. Phys*, *10*(13), 6311–6331, doi:10.5194/acp-10-6311-2010.

Lu, Z., Q. Zhang, and D. G. Streets (2011), Sulfur dioxide and primary carbonaceous aerosol emissions in China and India, 1996–2010, *Atmos. Chem. Phys*, *11*(18), 9839–9864, doi:10.5194/acp-11-9839-2011.

Massie, S. (1994), Indexes of Refraction for the HITran Compilation, *J. Quant. Spect. Radiat. Transfer*, *52*(3-4), 501–513.

Mätzler, C. (2002), MATLAB functions for Mie scattering and absorption, *IAP Res. Rep*, *8*.

Muller, D., U. Wandinger, and A. Ansmann (1999), Microphysical particle parameters from extinction and backscatter lidar data by inversion with regularization: Simulation, *Applied Optics*, *38*(12), 2358–2368.

Murphy, D. M., D. S. Thomson, and M. J. Mahoney (1998), In Situ Measurements of Organics, Meteoritic Material, Mercury, and Other Elements in Aerosols at 5 to 19 Kilometers, *Science*, *282*(5394), 1664–1669, doi:10.1126/science.282.5394.1664.

Murphy, D., D. Cziczo, P. Hudson, and D. S. Thomson (2007), Carbonaceous material in aerosol particles in the lower stratosphere and tropopause region, *J. Geophys. Res*, *112*, D04203.

Myhre, C., D. Christensen, F. Nicolaisen, and C. Nielsen (2003), Spectroscopic study of aqueous H2SO4 at different temperatures and compositions: Variations in dissociation and optical properties, *J Phys Chem A*, *107*(12), 1979–1991.

Neely, R. R., III, J. M. English, O. B. Toon, S. Solomon, M. Mills, and J. P. Thayer (2011), Implications of extinction due to meteoritic smoke in the upper stratosphere, *Geophys. Res. Lett*, *38*(24), doi:10.1029/2011GL049865.

Newhall, C., and S. Self (1982), The Volcanic Explosivity Index (Vei) - an Estimate of Explosive Magnitude for Historical Volcanism, *J. Geophys. Res*, *87*, 1231–1238.

O'Neill, N. T. et al. (2012), Properties of Sarychev sulphate aerosols over the Arctic, *J. Geophys. Res*, *117*(D4), D04203–, doi:10.1029/2011JD016838.

Palmer, K., and D. Williams (1975), Optical constants of sulfuric acid; application to the clouds of Venus? *Applied Optics*, *14*(1), 208–219, doi:10.1364/AO.14.000208. [online] Available from: http://www.opticsinfobase.org/abstract.cfm?uri=ao-14-1-208

Park, M., W. J. Randel, L. K. Emmons, and N. J. Livesey (2009), Transport pathways of carbon monoxide in the Asian summer monsoon diagnosed from Model of Ozone and Related Tracers (MOZART), *J. Geophys. Res*, *114*(D8), D08303, doi:10.1029/2008JD010621.

Prata, A. J., and C. Bernardo (2007), Retrieval of volcanic SO 2column abundance from Atmospheric Infrared Sounder data, *J. Geophys. Res*, *112*, D20204, doi:10.1029/2006JD007955.

Prata, A. J., G. Gangale, L. Clarisse, and F. Karagulian (2010), Ash and sulfur dioxide in the 2008 eruptions of Okmok and Kasatochi: Insights from high spectral resolution satellite measurements, *Journal of Geophysical Research-Atmospheres*, *115*, –, doi:10.1029/2009JD013556.

Prata, A., S. Carn, A. Stohl, and J. Kerkmann (2007), Long range transport and fate of a stratospheric volcanic cloud from Soufriere Hills volcano, Montserrat, *Atmospheric Chemistry and Physics*, *7*(19), 5093–5103.

Pumphrey, H. C. et al. (2007), Validation of middle-atmosphere carbon monoxide retrievals from the Microwave Limb Sounder on Aura, *J. Geophys. Res*, *112*(D24), D24S38, doi:10.1029/2007JD008723.

Redemann, J. et al. (2000), Retrieving the vertical structure of the effective aerosol complex index of refraction from a combination of aerosol in situ and remote sensing measurements during TARFOX, *Journal of Geophysical Research-Atmospheres*, *105*(D8), 9949–9970.

Rosenlof, K. H., and G. C. Reid (2008), Trends in the temperature and water vapor content of the tropical lower stratosphere: Sea surface connection, *J. Geophys. Res*, *113*, D06107, doi:10.1029/2007JD009109.

Smith, S. J., J. van Aardenne, Z. Klimont, R. J. Andres, A. Volke, and S. Delgado Arias (2011), Anthropogenic sulfur dioxide emissions: 1850–2005, *Atmos. Chem. Phys*,

11(3), 1101–1116, doi:10.5194/acp-11-1101-2011.

Thomas, H. E., I. M. Watson, C. Kearney, S. A. Carn, and S. J. Murray (2009), A multi-sensor comparison of sulphur dioxide emissions from the 2005 eruption of Sierra Negra volcano, Galápagos Islands, *Remote Sensing of Environment*, *113*(6), 1331–1342, doi:10.1016/j.rse.2009.02.019.

Tupper, A., I. Itikarai, M. Richards, F. Prata, S. Carn, and D. Rosenfeld (2007), Facing the Challenges of the International Airways Volcano Watch: The 2004/05 Eruptions of Manam, Papua New Guinea, *Wea. Forecasting*, *22*(1), 175–191, doi:10.1175/WAF974.1.

Vernier, J. P. et al. (2011), Major influence of tropical volcanic eruptions on the stratospheric aerosol layer during the last decade, *Geophys. Res. Lett*, *38*(12), L12807–, doi:10.1029/2011GL047563.

Waythomas, C. F., W. E. Scott, S. G. Prejean, D. J. Schneider, P. Izbekov, and C. J. Nye (2010), The 7–8 August 2008 eruption of Kasatochi Volcano, central Aleutian Islands, Alaska, *J. Geophys. Res*, *115*, B00B06, doi:10.1029/2010JB007437.

Yue, G. K., and A. Deepak (1982), Temperature dependence of the formation of sulfate aerosols in the stratosphere, *J. Geophys. Res*, *87*(C4), 3128–3134.

Zhao, F., Z. Gong, H. Hu, M. Tanaka, and T. Hayasaka (1997), Simultaneous determination of the aerosol complex index of refraction and size distribution from scattering measurements of polarized light, *Appl. Opts*, *36*(30), 7992–8001.